JOC The Journal of Organic Chemistry

Article

Cite This: J. Org. Chem. 2020, 85, 92−100

pubs.acs.org/joc

Benzo[*cd*]triangulene: A Spin 1/2 Graphene Fragment

Prince Ravat,*[,†,‡] Olivier Blacque,[§] and Michal Juríček*[,‡,§]

[†]Institute of Organic Chemistry, University of Würzburg, Am Hubland, D-97074 Würzburg, Germany

[‡]Department of Chemistry, University of Basel, St. Johanns-Ring 19, CH-4056 Basel, Switzerland

[§]Department of Chemistry, University of Zurich, Winterthurerstrasse 190, CH-8057 Zurich, Switzerland

Supporting Information

ABSTRACT: How does edge modification affect spin distribution in open-shell graphene fragments? We investigated this effect by analyzing spin-delocalization in benzo[*cd*]-triangulene, a spin 1/2 graphene fragment composed of seven benzenoid rings fused in a hybrid zigzag/armchair fashion. Six rings of this system form the core of Clar's hydrocarbon triangulene, to which an additional ring is annulated in the zigzag region. The singly occupied molecular orbital (SOMO) of this hydrocarbon radical resembles both SOMOs of triangulene, but the spin density is distributed over the core in a nonuniform fashion. The uneven spin distribution is reflected in the reactivity—reaction with oxygen occurs selectively at a position with the highest spin density—and correlates nicely with relative stabilities of the corresponding Clar resonance structures. The spin distribution is different from that of a topologically similar compound composed of the same number of sp^2 carbon atoms but featuring six rings only, illustrating the impact of subtle structural changes on spin-density distribution. This compound was characterized by means of UV−vis and electron paramagnetic resonance spectroscopy, cyclic voltammetry, mass spectrometry, and X-ray crystallography. The experimental results are supported by density functional theory calculations.

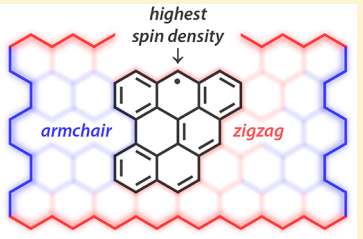

INTRODUCTION

Open-shell triangular graphene[1] fragments containing one or more unpaired electrons delocalized around the zigzag edges[2] are long sought for potential applications in spintronics[3] and as molecular cubits[4] for quantum computing.[5] The smallest member of this class of compounds is phenalenyl[6] (**1**; Figure 1, left), a spin 1/2 odd-alternant three-ring hydrocarbon, characterized by a uniform distribution of the electron spin density around the periphery. Parent phenalenyl is stable in oxygen-free solutions,[7] where it exists in an equilibrium with its σ dimer.[8] Substituted phenalenyls analyzed by single-crystal X-ray diffraction were found to form either σ or π dimers in the solid state depending on the crystallization conditions and the steric bulk of substituents, which can partially or fully suppress σ dimerization.[9]

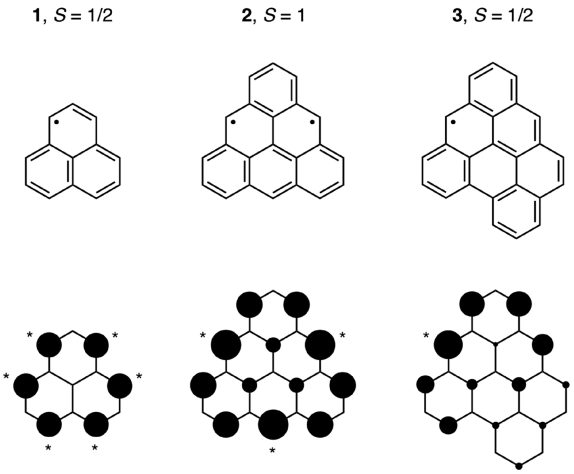

Figure 1. (top) Structures of phenalenyl (**1**; left), triangulene (**2**; middle), and benzo[*cd*]triangulene (**3**; right) and (bottom) the corresponding positive electron spin densities obtained from HMO calculations. Positions that display the highest spin density in each molecule are marked with an asterisk.

The second homologue in this series is triangulene[10] (**2**; Figure 1, middle), a diradical molecule composed of six benzenoid rings, known as Clar's hydrocarbon. A special feature of this even-alternant non-Kekulé system is its triplet ground state (S = 1). Although unsubstituted triangulene has not yet been isolated on account of its high reactivity, the triplet ground state could be validated for its trisubstituted derivative.[11] Similarly to phenalenyl, spin density in triangulene is distributed mostly around the periphery. In contrast to phenalenyl, however, the peripheral positions in triangulene are not equal, and the highest spin density is displayed by the carbon atoms in the middle of the zigzag edges.

As a consequence of spin concentration at the peripheral carbon atoms, phenalenyl, triangulene, and their extended homologues are highly reactive. They readily unite with dioxygen as well as undergo dimerization[9] and oligomerization[10,11] at the peripheral positions. Positions that display the highest spin density (marked with * in Figure 1) are, in

Special Issue: Functional Organic Materials

Received: August 6, 2019
Published: October 7, 2019

DOI: 10.1021/acs.joc.9b02163
J. Org. Chem. 2020, 85, 92−100

principle, more reactive than those with less spin concentration, which can result in selective reactivity. Control over the spin distribution in such systems could therefore enable their use as synthetic building blocks for accessing larger open-shell graphene nanostructures.

Fusion of additional ring(s) changes the topology of an open-shell system, which can alter the number of unpaired electrons and the shape of the singly occupied molecular orbital(s) (SOMO). Using topology, one can thus manipulate spin distribution by design. In this work, we examined this strategy in a system obtained by fusion of one benzenoid ring in the zigzag edge of triangulene, yielding a hybrid zigzag/armchair spin 1/2 graphene fragment, namely, benzo[*cd*]-triangulene (**3**; Figure 1, right). According to the Hückel molecular orbital (HMO) analysis, spin distribution in **3** is highly nonuniform, and in contrast to phenalenyl and triangulene, the highest spin density in **3** is displayed only by one zigzag carbon atom. Further inspection of the HMO results reveals that the SOMO of **3** is similar to both SOMOs of triangulene, with less degree of uniformity within the triangulene subunit induced by the extra ring (Figure 2b,c).

This relationship is more obvious when **3** is viewed as an extension of spin 1/2 fragments of triangulene **4** and **5** (Figure 2a), the SOMOs of which are topologically identical to triangulene's SOMO-1 and SOMO-2, respectively. Below, we report the synthesis of a derivative of **3** equipped with four phenyl substituents around the periphery (**3a**; Scheme 1) and investigation of its spin distribution, properties, and reactivity by experimental (electron paramagnetic resonance (EPR), UV−vis, cyclic voltammogram (CV), X-ray diffraction (XRD)) and theoretical (density functional theory (DFT)) means.

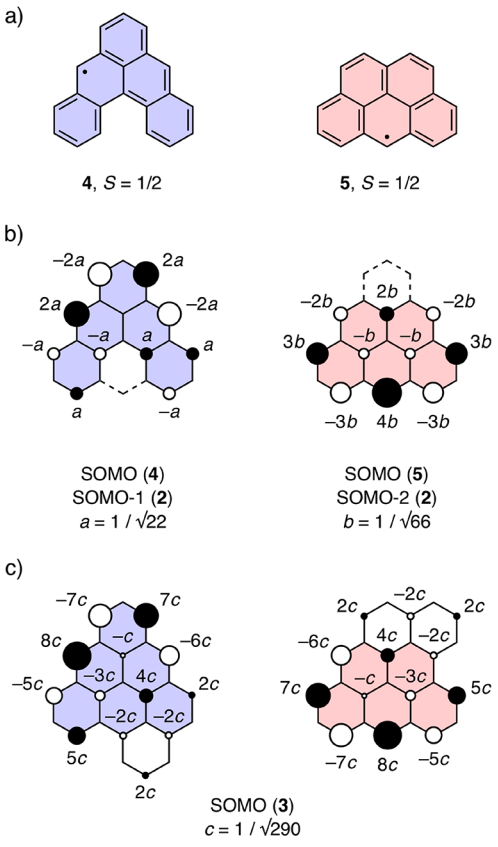

Figure 2. (a) Structures of spin 1/2 triangulene subunits **4** (blue) and **5** (red), each possessing a SOMO that is topologically identical to (b) SOMO-1 and SOMO-2, respectively, of triangulene (**2**). (c) SOMO of **3** in two different orientations, illustrating its reminiscence to both SOMOs of triangulene. The SOMOs shown with the corresponding coefficients (expressed as multiples of *a*, *b*, and *c*) were obtained from HMO calculations.

RESULTS AND DISCUSSION

Synthesis and Characterization. Tetraphenyl benzotriangulene **3a** was synthesized in six steps starting from a [5]helicene[12] precursor **6** reported previously[13] (Scheme 1). Precursor **6** is equipped with three phenyl substituents and a bromomethyl group, which allowed for elongation of the chain by two carbon atoms via (1) S_N2 reaction with a lithium salt of methyl 2-phenylacetate (yielding crude ester **7**), (2) hydrolysis of the ester moiety (yielding crude acid **8**), and (3) acyl chloride formation and Friedel−Crafts acylation providing intermediate **9** in 53% yield over the three steps. In addition to ring-closure during the Friedel−Crafts step, fusion of the [5]helicene unit in the fjord region occurred[14] (the formed bond is highlighted in bold in Scheme 1). This unexpected reaction was observed, while we were working on the synthesis of helically chiral open-shell graphene fragments,[13,15] and inspired us to synthesize **3a**. The structure of compound **9** was confirmed by two-dimensional (2D) NMR spectroscopy including COSY, NOESY, HMQC, and HMBC. Subsequent reduction of ketone **9** and dehydration gave the hydro-precursor **11** in 59% yield over the two steps.

The hydroprecursor **11** was oxidized with *p*-chloranil in dichloromethane (DCM) at room temperature in a glovebox with a nitrogen atmosphere. The resulting dark orange−red solution of **3a** in DCM was diluted with *n*-hexane to precipitate out 2,3,5,6-tetrachlorobenzene-1,4-diol that was filtered through a syringe filter. Removal of the solvent gave **3a** as a red solid in 83% yield. When exposed to air, the dark orange−red solution of **3a** in DCM or toluene changes to pale orange due to oxidation. Noticeably, only a single oxidation product, compound **12**, could be isolated in 69% yield upon purification of the oxidized sample by column chromatography. If other oxidation products were formed, these must have been present in very small quantities only as they could not be isolated. The structure of **12** was confirmed by 2D NMR spectroscopy, and solid-state structures for both **3a** and **12** were validated by single-crystal X-ray analysis.

Single crystals of **3a** were grown by a slow diffusion of *n*-hexane into a solution of **3a** in DCM in a glovebox. The obtained dark red crystals were analyzed by single-crystal XRD, which revealed that **3a** crystallized in a non-centrosymmetric monoclinic $P2_1/c$ space group. The asymmetric unit contains one molecule of **3a** and 0.2 molecule of the crystallization solvent *n*-hexane (Figure 3a). The benzotriangulene core of **3a** slightly deviates from planarity, and the phenyl groups are noncoplanar with respect to the core.

Analysis of the crystal packing did not show presence of π-dimers, which is commonly observed for spin-delocalized systems. Instead, slipped molecular stacks arranged in a herringbone fashion were formed (Figure S1). This packing mode can be, at least in part, the result of the steric hindrance effect of the four phenyl substituents.

Single crystals of **12** were grown by slow evaporation of solution of **12** in $CDCl_3$ in an NMR tube. The XRD analysis performed on the obtained orange crystals revealed a non-centrosymmetric monoclinic $P2_1/c$ space group, as in the case

DOI: 10.1021/acs.joc.9b02163
J. Org. Chem. 2020, 85, 92−100

Scheme 1. Synthesis of Benzotriangulene 3a and its Selective Oxidation in Air

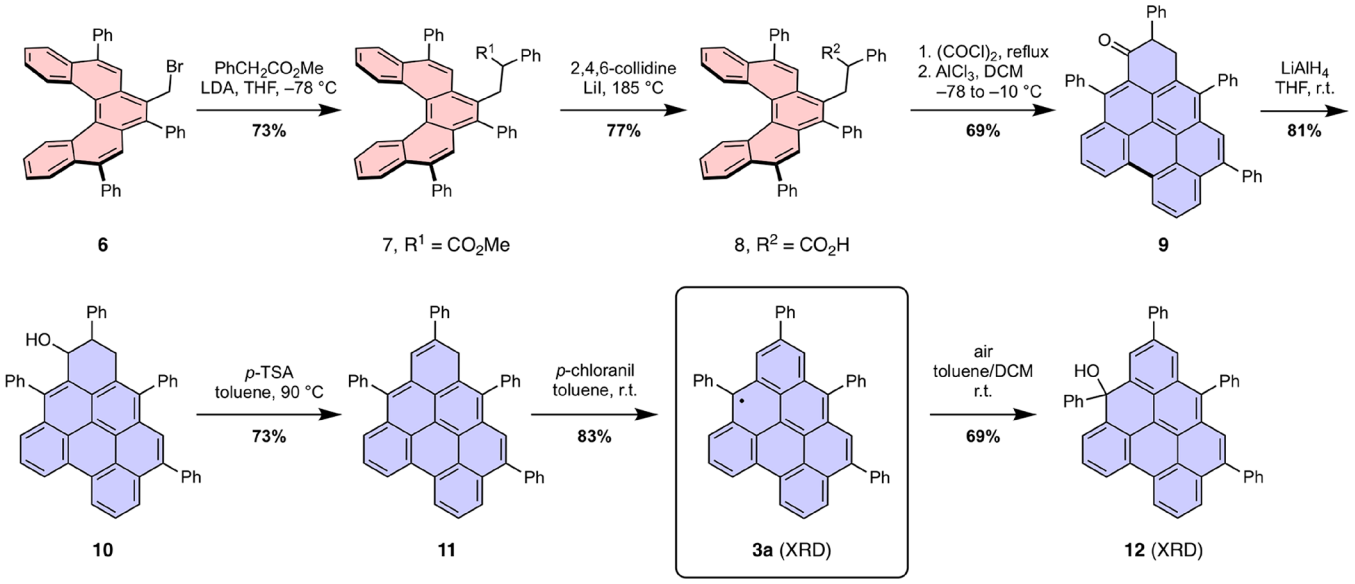

of **3a**. The asymmetric unit contains only one molecule of **12** (Figure 3b) and no solvent molecules. The out-of-plane distortion of the benzotriangulene core of **12** is more pronounced when compared to **3a**, as a result of the sp^3 hybridization of one of the core carbon atoms, which carries the OH group. This solid-state structure confirms that the oxidation of **3a** occurred predominantly at the position with the highest spin density (marked with * in Figure 1).

EPR Spectroscopy. The paramagnetic nature of compound **3a** was studied by means of EPR spectroscopy. A solution of **3a** in toluene (1×10^{-4} M) gave a well-resolved seven-line EPR spectrum at a g value of 2.0037 at 300 K (Figure 4). The obtained g value for **3a** is typical of delocalized spin 1/2 hydrocarbon radicals. From the measured EPR spectrum, four proton hyperfine coupling constants (hcc) of ~4.0 (2×) and 6.6 G (2×) were elucidated. The hcc values for all protons of **3a** (Figure 5, top left) were obtained from DFT calculations (UM05-2X/EPR-III) performed on the optimized geometry (UB3LYP/6-31G(d,p)). While the protons attached directly to the benzotriangulene core possess the largest hcc values in accord with spin-density distribution (Figure 5, top right), the protons of phenyl substituents possess much smaller hcc values (Table S2). Because of the presence of five nonequivalent core protons displaying hcc values in the range of 1.0−1.7 G, only the four highest hcc values in the range of 4.0−6.6 G could be elucidated from our experimental data (Figure 4). These four couplings, two 4.0 G in magnitude and two 6.6 G in magnitude, account for the observed seven-line signal and are in agreement with the highest calculated hcc values (6.6, 6.4, 3.8, and 3.8 G). In addition, the signal width (w) of ~27.6 G agrees well with the sum of the core hcc values (26.6 G). When the sample temperature decreases (Figure 4), intensity of the EPR signal increases, following the Curie law (Figure S3). This observation suggests that the phenyl substituents suppress both the σ- and π-dimer formation in toluene.[9b,16]

Clar Resonance Structures. The HMO (Figure 1) and DFT (Figure 5) calculations as well as EPR spectroscopy (Figure 4) corroborate the nonuniform spin distribution in **3a**, which, in comparison to phenalenyl and triangulene, is less uniform because of symmetry breaking. The nonuniform spin distribution can be rationalized qualitatively by evaluation of the relative stabilities of Clar resonance structures of **3a** (Figure 6b). It is a general practice to compare the relative stabilities of isomeric polycyclic aromatic hydrocarbons by the number of Clar's sextets[17] in the most stable Clar resonance structure, textbook examples being anthracene (one Clar's sextet, less stable) and phenanthrene (two Clar's sextets, more stable). This approach gives three main classes of Clar resonance structures for **3a**, namely, structures with three, two, or one Clar's sextets. The structure with the highest and the lowest number of Clar's sextets will result in the highest or the lowest positive Mulliken spin densities (msd) values, respectively, at positions, where the unpaired electron resides in the corresponding resonance structure: msd = 0.41−0.32 for three, 0.22−0.08 for two, and 0.07−0.05 for one Clar's sextet. In addition, each main class can be subcategorized based on the number of aromatic rings, where the Clar's sextet can migrate (blue-filled), and then further based on the number of aromatic rings with a localized double bond (red-filled). As shown in Figure 6b, the relative stabilities of Clar resonance structures evaluated in this way are in perfect qualitative agreement with the calculated positive msd values. On the basis of this analysis, and in accord with HMO and DFT calculations, the highest spin density is at the position with msd = 0.41 (Figure 6, top left). In accord with these considerations, **3a** reacts with dioxygen selectively at the position with the highest spin density to give the hydroxy compound **12** as the major product (Scheme 1), which demonstrates the power of the predictions based on the analysis of Clar resonance structures.

This analysis is in a good qualitative agreement with the trend observed for the aromatic character of individual benzenoid rings assessed through the NICS(1) values (Figure 6a) obtained from DFT calculations at the GIAO-B3LYP/6-31G(d,p) level on B3LYP/6-31G(d,p) geometries. The NICS(1) values show that the aromatic character of individual rings decreases in the order G > C ≈ D > A ≈ F > B ≈ E. To some degree, this trend is nicely reflected by the most contributing resonance structure (Figure 6b, top left), where

DOI: 10.1021/acs.joc.9b02163
J. Org. Chem. 2020, 85, 92−100

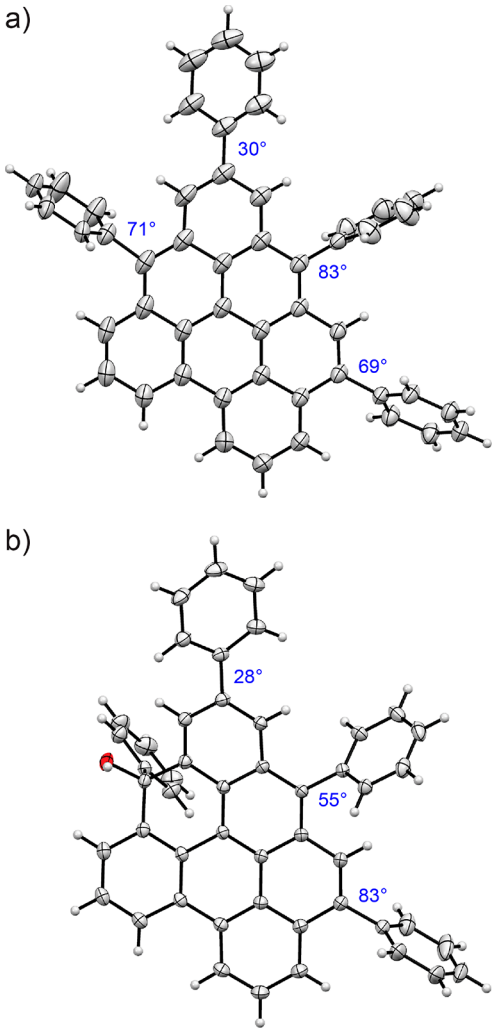

Figure 3. Solid-state structures of (a) **3a** and (b) **12**. Thermal ellipsoids are shown at a 50% probability level. Dihedral angles between the mean planes of the phenyl rings and the core are shown in blue. The oxygen atom of the OH group of **12** is shown in red. Solvent molecule and disorder of one Ph group in **3a** are omitted for clarity.

rings G and D have one Clar's sextet each, rings C and A share one migrating Clar's sextet, ring F has a localized double bond, ring B has an unpaired electron, and ring E is empty. A more accurate picture is obtained when the relative contribution of each resonance structure is accounted for. Then, it becomes clear that ring G with the lowest NICS(1) value of −26.1 is the most aromatic (Clar's sextet is in every but one resonance structure) and ring E with the highest NICS(1) value of −2.7 is the least aromatic (empty ring in every but one resonance structure).

It is noteworthy to make a comparison between **3a** and its helical analogue **13** that we reported[13] previously (Figure 7). Although the cores of these two compounds are topologically similar, they differ in the number of fused benzenoid rings (seven in **3a** vs six in **13**) and shape (planar **3a** vs helical **13**). This structural difference is reflected in the distribution of the spin density, which is less nonuniform around the phenalenyl subunit in the case of **13** (msd values in the range of 0.37−0.27 in contrast to **3a** with msd values in the range of 0.41−0.22). This difference can be understood by looking at the structural relationship of **3a** and **13** to spin 1/2 triangulene subunits **4** and **5**. While the core of **3a** represents an extension of both subunits, the core of **13** is only an extension of **4**, and the spin distribution of **13** thus reflects the spin distribution of **4** more than does that of **3a**. The less nonuniform spin distribution of the core of **13** is also reflected in the reactivity. A monosubstituted derivative of **13**, bearing a phenyl substituent at the position with msd = 0.27, which sterically hinders the position with msd = 0.32, was found to give upon exposure to dioxygen two keto products, one with oxygen attached at position with msd = 0.37 (major) and one at msd = 0.35 (minor). This result nicely illustrates the effect of subtle changes in spin distribution on reaction selectivity.

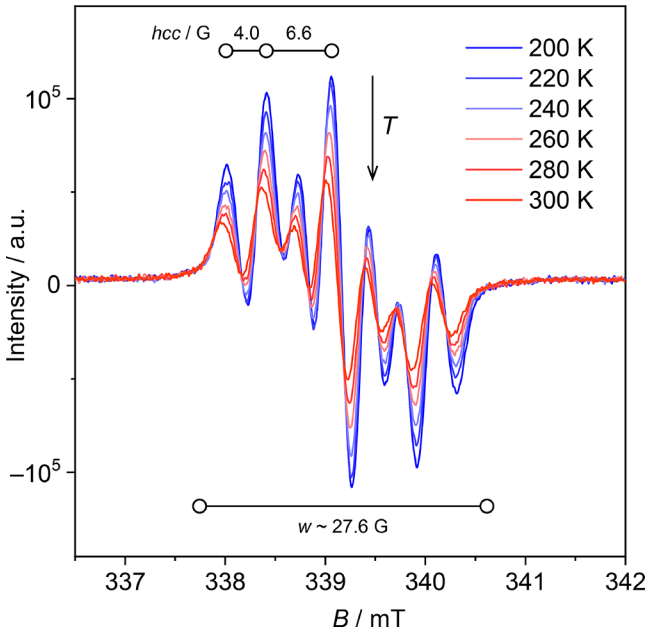

Figure 4. Variable-temperature EPR spectra of **3a** (toluene, 1×10^{-4} M) recorded in the temperature range of 200−300 K (hcc = proton hyperfine coupling constant, w = signal width).

UV−Vis Spectroscopy. The UV−vis spectrum of **3a** in DCM displays an absorption maximum at 553 nm, corresponding to the SOMO-α to LUMO-α (LUMO = lowest unoccupied molecular orbital) transition (Figure 8), which is significantly red-shifted in comparison to phenalenyl (325 nm, time-dependent (TD) DFT-calculated). The measured UV−vis spectrum is well-reproduced by TD-DFT calculations at the UB3LYP/6-31G(d,p) level. The calculated SOMO-α−LUMO-α energy gap of **3a** (2.64 eV) is significantly lower than that of phenalenyl (4.18 eV), which can be attributed to extended π-conjugation. This results in the bathochromic shift of SOMO-α−LUMO-α transition in the UV−vis spectrum. Similarly, to spin-density distribution, the shape of the frontier molecular orbitals, the SOMO and the LUMO, is also nonuniform, SOMO being more localized on one-half of the molecule, while the LUMO is on the other half (Figure 5, bottom left and right, respectively).

Cyclic Voltammetry. The CV measurement confirmed the anticipated amphoteric redox ability of **3a**, originating from the presence of a nonbonding molecular orbital (NBMO). The CV plot of **3a** in tetrahydrofuran (THF) consists of two reversible, one oxidation (E_{ox}) and one reduction (E_{red}), waves at 0.01 and −1.35 V, respectively, versus Fc/Fc^+ (Figure 9). From the oxidation wave, the energy of the SOMO was calculated to be −4.78 eV. While the E_{red} value of **3a** is similar to that of

DOI: 10.1021/acs.joc.9b02163
J. Org. Chem. 2020, 85, 92−100

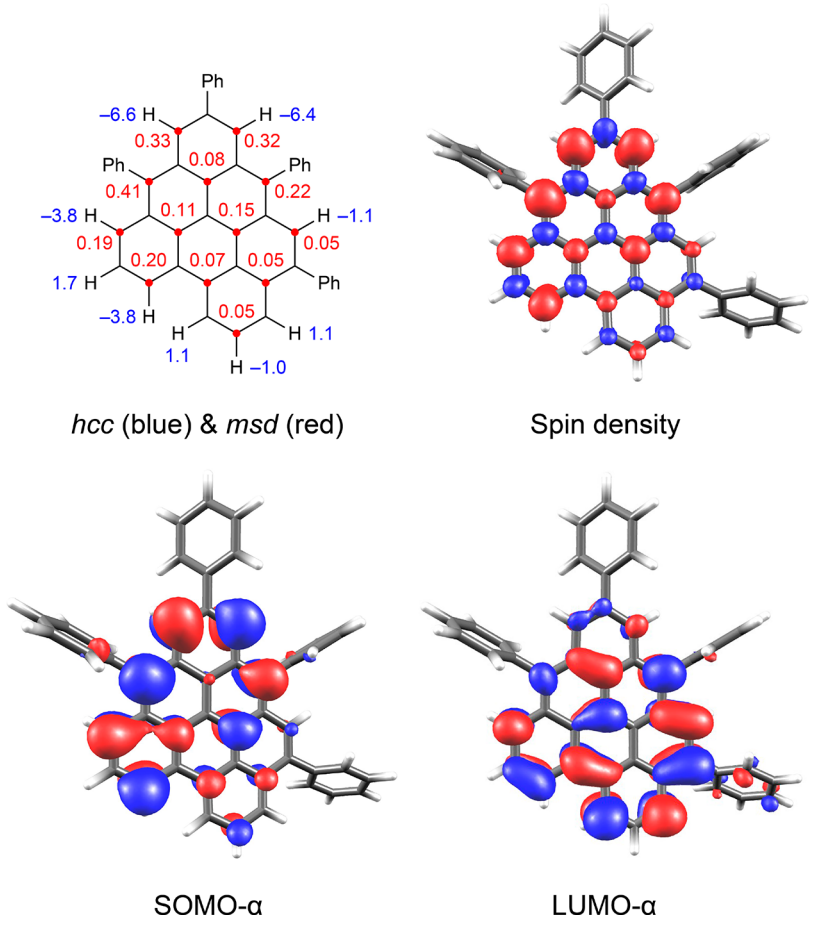

Figure 5. DFT-Calculated proton hcc (in blue; UM05-2X/EPR-III on UB3LYP/6-31G(d,p) geometry) and positive msd (in red; UB3LYP/6-31G(d,p)) of the benzotriangulene core (top left). Spin-density distribution (top right) and frontier molecular orbitals of **3a**, SOMO-α (bottom left) and LUMO-α (bottom right), obtained from DFT calculations (UB3LYP/6-31G(d,p)).

phenalenyl and its derivatives[9b] (ca. −1.30 eV), the E_{ox} value is significantly decreased because of extended π-conjugation. This leads to a smaller E_g ($E_g = E_{ox} - E_{red}$) value of 1.36 V compared to that of phenalenyl (1.6 V). The E_g value also corresponds to the pairing energy required to place a second electron in the SOMO, the magnitude of which represents the on-site Coulomb repulsion energy (U).[18] The smaller value of U is desired for increasing the conductivity of a material.

CONCLUSION

In summary, we synthesized and fully characterized a tetraphenyl derivative of a spin 1/2 graphene fragment benzo[*cd*]triangulene, compound **3a**. The unsymmetrical structure of **3a** results in a nonuniform spin distribution, which is reflected in selective reactivity and which can be rationalized simply by considering the relative stabilities of Clar resonance structures, in accord with HMO and DFT calculations. The lesson learned from investigation of this molecule can be used in the design of open-shell graphene fragments and to control their reactivity through the *edge design* that governs the spin distribution.

EXPERIMENTAL SECTION

Materials and Instrumentation. All chemicals and solvents were purchased from commercial sources and were used without further purification unless stated otherwise. The reactions and experiments that are sensitive to dioxygen were performed using Schlenk techniques and argon-saturated solvents. The NMR experiments were performed on NMR spectrometers operating at 400 or 500 MHz proton frequencies. Standard pulse sequences were used, and the data were processed using twofold zero-filling in the indirect dimension for all 2D experiments. Chemical shifts (δ) are reported[19] in parts per million (ppm) relative to the solvent residual peak (^{1}H and ^{13}C NMR, respectively): $CDCl_3$ (δ = 7.26 and 77.16 ppm) and CD_2Cl_2 (δ = 5.32 and 53.84 ppm). The UV−vis spectra were recorded in DCM at room temperature. The EPR spectra were recorded in an argon-saturated toluene (~1 × 10^{-4} M, unless stated otherwise) on an X-band continuous wave (CW) EPR spectrometer (9.66 GHz), equipped with a variable temperature-control continuous-flow-N_2 cryostat. The *g*-factor corrections were obtained by using 2,2-diphenyl-1-picrylhydrazyl (DPPH) (g = 2.0037) as a standard.

(±)-Methyl 2-phenyl-3-(1,4,6-triphenyldibenzo[c,g]phenanthren-3-yl)propanoate (7). A solution of lithium diisopropylamide (LDA) (8.5 mL, 17 mmol, 2 M in THF/heptane) was added dropwise to a cooled (−78 °C) solution of methyl 2-phenylacetate (1.95 g, 12.5 mmol) in dry THF (50 mL) under an argon atmosphere. The reaction mixture was stirred at −78 °C for 2 h before a suspension of **6** (600 mg, 1.00 mmol) in dry THF (40 mL) was added dropwise at −78 °C. The reaction was then allowed to warm to room temperature overnight before saturated aqueous NH_4Cl (25 mL) was added to quench the reaction. The reaction mixture was extracted with CH_2Cl_2 (4 × 25 mL), and the combined organic layers were washed with brine, dried over anhydrous Na_2SO_4, and filtered. After evaporation of the solvents, the residue was purified by column chromatography over silica gel using cyclohexane/CH_2Cl_2 (4:1) as an eluent to afford the desired product (489 mg, 73%) as a yellow solid and as an ~1:1 mixture of two possible of diastereomers.

DOI: 10.1021/acs.joc.9b02163
J. Org. Chem. 2020, 85, 92−100

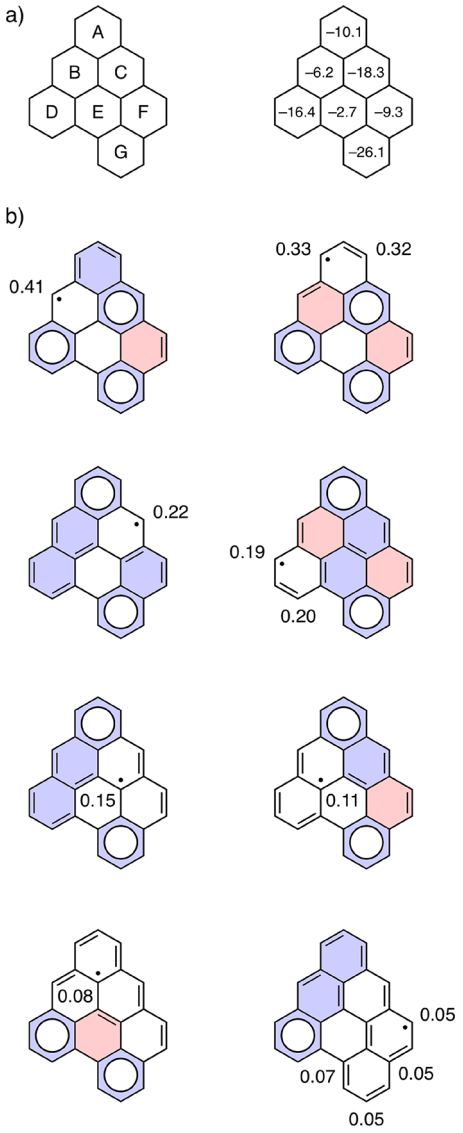

Figure 6. (a) Annotation of rings and the corresponding NICS(1) values obtained by DFT at the GIAO-B3LYP/6-31G(d,p) level on B3LYP/6-31G(d,p) geometries. (b) Clar resonance structures of **3a** featuring three types of aromatic rings: (1) rings with Clar's sextet/blue-filled with a white-filled circle, (2) rings, where Clar's sextet can migrate to/blue-filled, (3) rings with a localized double bond/red-filled. Numbers indicate the positive msd values at the corresponding positions (see Figure 5), which correlate with the relative stability of the Clar resonance structures.

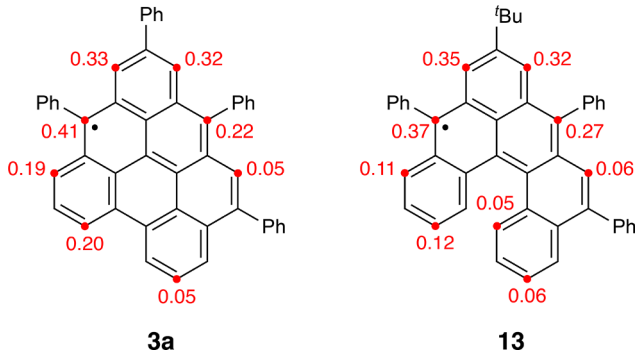

Figure 7. Comparison of the peripheral positive msd values for **3a** and its helical analogue **13** (DFT/UB3LYP/6-31G(d,p)).

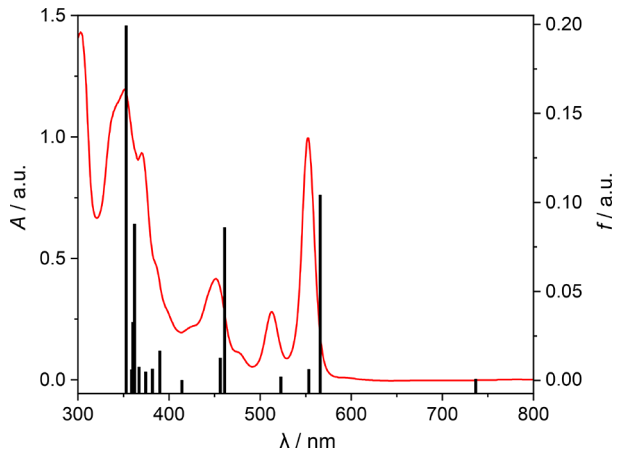

Figure 8. Measured (red line; DCM, 8.1 × 10^{-5} M, 25 °C) and calculated (black vertical lines; TD-DFT/UB3LYP/6-31G(d,p)) UV−vis spectra of **3a**. f = oscillator strength.

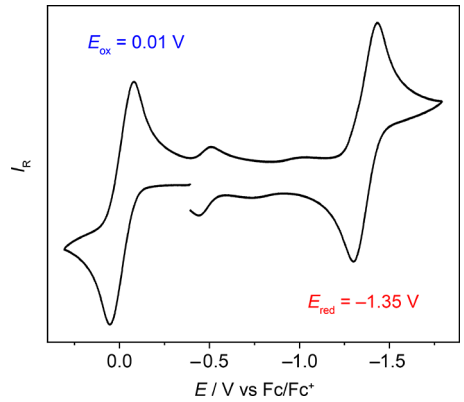

Figure 9. CV plot of **3a** vs ferrocene(Fc)/ferrocenium(Fc^+) at a scan rate of 50 mV s^{-1} in THF with a supporting electrolyte [Bu_4N][PF_6] (0.1 M).

The product obtained this way contained unknown impurities, which did not allow a reliable reporting of ^{13}C NMR data, and it was used in the next step without further purification. ^1H NMR (400 MHz, $CDCl_3$, ppm): δ 8.53 (d, J = 8.5 Hz, 1H), 8.50 (d, J = 8.5 Hz, 1H), 8.01 (dd, J = 8.4, 1.3 Hz, 1H), 7.96 (s, 1H), 7.91 (dd, J = 8.3, 1.3 Hz, 1H), 7.75−7.68 (m, 2H), 7.59 (dd, J = 7.5, 7.5 Hz, 2H), 7.54−7.24 (m, 15H), 7.12−7.02 (m, 3H), 6.97−6.84 (m, 3H), 3.94 (dd, J = 6.8, 6.5 Hz, 1H), 3.86 (dd, J = 14.3, 6.1 Hz, 1H), 3.50 (dd, J = 14.3, 7.4 Hz, 1H), 3.44 (s, 3H). High-resolution mass spectrometry (HRMS) (electrospray ionization time-of-flight (ESI-TOF)) m/z: $[M + Na]^+$ Calcd for $C_{50}H_{36}O_2Na$ 691.2608; Found 691.2600.

*(±)-2-Phenyl-3-(1,4,6-triphenyldibenzo[c,g]phenanthren-3-yl)-propanoic Acid (**8**).* A mixture of **7** (0.45 g, 0.67 mmol), lithium iodide (631 mg, 4.71 mmol), and 2,4,6-collidine (10 mL) was heated at 185 °C for 2 h under an argon atmosphere before the reaction mixture was cooled to room temperature and concentrated in vacuum. To the residue, aqueous HCl (30 mL, 2 M) was added, and the precipitate that formed was filtered and washed with water to afford the desired product (338 mg, 77%) as a brown solid and as an ∼1:1 mixture of two possible diastereomers. The product obtained this way contained ∼30% of 2,4,6-collidine, which did not allow a reliable reporting of ^{13}C NMR data, and was used in the next step without further purification. ^1H NMR (400 MHz, CD_2Cl_2, ppm): δ 8.56−8.46 (m, 2H), 8.20 (s, 0.5H), 8.03 (d, J = 8.2 Hz, 1H), 8.02 (s, 0.5H), 7.94 (2 × d, J = 8.6 Hz, 1H), 7.76−7.67 (m, 2H), 7.59 (2 × dd, J = 7.5, 7.5 Hz, 2H), 7.55−7.08 (m, 18H), 6.98 (2 × d, J = 7.5 Hz, 2H), 6.91 (d, J = 7.0 Hz, 0.5H), 6.84 (d, J = 7.0 Hz, 0.5H), 4.11−3.88

DOI: 10.1021/acs.joc.9b02163
J. Org. Chem. 2020, 85, 92−100

(m, 2H), 3.60−3.41 (m, 1H). HRMS (ESI-TOF) m/z: $[M + Na]^+$ Calcd for $C_{49}H_{34}O_2Na$ 677.2451; Found 677.2449.

*(±)-7,9,11,13-Tetraphenyl-9,10-dihydro-8H-naphtho[3,2,1,8-pqra]perylen-8-one (**9**).* A solution of **8** (0.24 g, 0.36 mmol) in oxalyl chloride (15 mL) was heated at reflux for 2.5 h, before the excess of oxalyl chloride was removed under the reduced pressure. The crude acid chloride intermediate was dissolved in CH_2Cl_2 (100 mL), and the solution was cooled to −78 °C. Solid $AlCl_3$ (169 mg, 1.27 mmol) was added, and the reaction mixture was allowed to warm to −10 °C over 5 h, before it was poured onto ice and acidified with aqueous HCl (2 M). The organic layer was separated, and the aqueous layer was extracted with CH_2Cl_2. The combined organic layers were washed with saturated aqueous $NaHCO_3$, water, and brine, dried over anhydrous Na_2SO_4, and filtered. After evaporation of the solvents, the residue was purified by column chromatography over silica gel using cyclohexane/CH_2Cl_2 (7:3) as an eluent to afford the desired product (160 mg, 69%) as a yellow solid. mp 259−261 °C. ^{1}H NMR (500 MHz, CD_2Cl_2, ppm): δ 9.16 (d, J = 7.7 Hz, 1H), 9.11 (d, J = 7.8 Hz, 1H), 8.23 (d, J = 8.0 Hz, 1H), 8.01 (dd, J = 7.9, 7.9 Hz, 1H), 7.96 (dd, J = 7.9, 7.9 Hz, 1H), 7.85 (d, J = 8.1 Hz, 1H), 7.70 (s, 1H), 7.62−7.44 (m, 12H), 7.41−7.37 (m, 1H), 7.30−7.26 (m, 1H), 7.26−7.13 (m, 6H), 4.36 (dd, J = 9.1, 5.8 Hz, 1H), 3.82 (dd, J = 16.6, 9.1 Hz, 1H), 3.72 (dd, J = 16.7, 5.8 Hz, 1H). ^{13}C{^{1}H} NMR (101 MHz, CD_2Cl_2, ppm): δ 199.7, 141.26, 141.25, 140.4, 140.2, 139.7, 138.0, 137.9, 132.7, 131.1, 130.7, 130.5, 130.43, 130.40, 130.2, 129.9, 129.8, 129.31, 129.27, 128.8, 128.74, 128.65, 128.6, 128.51, 128.45, 128.3, 128.2, 128.0, 127.43, 127.42, 127.2, 127.1, 127.0, 126.7, 126.6, 126.1, 126.0, 123.5, 123.1, 122.6, 121.7, 55.4, 36.0. Unless there is signal overlap, 43 signals indicate three fast and one slow (most likely 7-Ph) rotations of the Ph substituents around the respective single bonds relative to the NMR time scale. HRMS (ESI-TOF) m/z: $[M + H]^+$ Calcd for $C_{49}H_{31}O$ 635.2369; Found 635.2363.

*(±)-7,9,11,13-Tetraphenyl-9,10-dihydro-8H-naphtho[3,2,1,8-pqra]perylen-8-ol (**10**).* A mixture of **9** (0.13 g, 0.20 mmol) and $LiAlH_4$ (23 mg, 0.61 mmol) in dry THF (10 mL) was stirred at room temperature for 45 min under an argon atmosphere, before the reaction was quenched by the addition of ice and aqueous HCl (10 mL, 2 M). The organic layer was separated, and the aqueous layer was extracted with CH_2Cl_2. The combined organic layers were washed with brine, dried over anhydrous Na_2SO_4, and filtered. Evaporation of the solvents afforded the desired product (106 mg, 81%) as a brown solid and as one, presumably the *cis*, of the two possible diastereomers. mp 290 °C dec. ^{1}H NMR (400 MHz, CD_2Cl_2, ppm): δ 9.15 (dd, J = 8.0, 1.1 Hz, 1H), 9.13 (dd, J = 8.0, 1.1 Hz, 1H), 8.22 (dd, J = 8.0, 1.1 Hz, 1H), 8.00 (dd, J = 7.9, 7.9 Hz, 1H), 7.95 (dd, J = 7.9, 7.9 Hz, 1H), 7.73 (dd, J = 8.0, 1.0 Hz, 1H), 7.67 (s, 1H), 7.65−7.42 (m, 15H), 7.38−7.32 (m, 2H), 7.32−7.26 (m, 2H), 7.24−7.17 (m, 1H), 5.05 (ddd, J = 3.5, 1.5, 1.5 Hz, 1H), 3.90 (dd, J = 16.2, 13.5 Hz, 1H), 3.45 (ddd, J = 13.5, 4.0, 2.0 Hz, 1H), 3.10 (ddd, J = 16.2, 4.0, 1.2 Hz, 1H), 1.84 (d, J = 3.9 Hz, 1H). ^{13}C{^{1}H} NMR (101 MHz, CD_2Cl_2, ppm): δ 142.9, 141.3, 140.1, 139.5, 138.9, 138.6, 137.3, 133.5, 132.5, 132.2, 130.9, 130.8, 130.51, 130.49, 130.46, 130.4, 130.3, 128.9, 128.82, 128.77, 128.7, 128.6, 128.5, 128.2, 127.9, 127.6, 127.5, 127.0, 126.6, 126.5, 126.3, 126.09, 126.06, 125.8, 125.4, 124.1, 123.8, 122.5, 121.2, 121.1, 70.3, 45.8, 29.0. Unless there is signal overlap, 43 signals indicate three fast and one slow (most likely 7-Ph) rotations of the Ph substituents around the respective single bonds relative to the NMR time scale. HRMS (ESI-TOF) m/z: $[M + Na]^+$ Calcd for $C_{49}H_{32}ONa$ 659.2345; Found 659.2347.

*7,9,11,13-Tetraphenyl-10H-naphtho[3,2,1,8-pqra]perylene (**11**).* *p*-Toluenesulfonic acid monohydrate (9 mg, 0.05 mmol) was added to a hot (90 °C) solution of **10** (0.10 g, 0.16 mmol) in toluene (10 mL), and the reaction mixture was heated at 90 °C for 5 min before it was cooled in an ice bath and passed through a pad of silica gel using toluene as an eluent to afford the desired product (71 mg, 73%) as a pale yellow solid. ^{1}H NMR (500 MHz, CD_2Cl_2, ppm): δ 9.10 (d, J = 8.2 Hz, 1H), 9.00 (d, J = 8.3 Hz, 1H), 8.19 (dd, J = 7.9, 1.0 Hz, 1H), 7.99 (dd, J = 7.9, 7.9 Hz, 1H), 7.88 (dd, J = 7.9, 7.9 Hz, 1H), 7.72 (dd, J = 7.9, 1.0 Hz, 1H), 7.68−7.62 (m, 4H), 7.62 (s, 1H), 7.61−7.43 (m, 11H), 7.34−7.21 (m, 5H), 7.06 (t, J = 1.8 Hz, 1H), 4.33 (d, J = 1.8 Hz, 2H). ^{13}C{^{1}H} NMR (101 MHz, CD_2Cl_2, ppm): δ 141.5, 140.5, 140.1, 139.9, 139.5, 137.7, 137.6, 135.3, 133.6, 131.5, 131.2, 130.9, 130.73, 130.72, 130.5, 130.2, 129.83, 129.80, 129.2, 128.84, 128.77, 128.5, 128.2, 128.01, 127.97, 127.9, 126.8, 126.5, 126.4, 126.06, 126.05, 125.7, 125.6, 125.4, 124.4, 123.1, 122.7, 122.3, 121.5, 120.7, 34.4. Unless there is signal overlap, 41 signals indicate fast rotation of all four Ph substituents around the respective single bonds relative to the NMR time scale. HRMS (ESI-TOF) m/z: $[M - H]^+$ Calcd for $C_{49}H_{29}$ 617.2264; Found 617.2255.

*7,9,11,13-Tetraphenylnaphtho[3,2,1,8-pqra]perylene or 7,9,11,13-tetraphenylbenzo[cd]-triangulene (**3a**).* To a solution of **11** (16 mg, 0.027 mmol) in DCM (3 mL), *p*-chloranil (4.5 mg, 0.019 mmol) was added at room temperature in a glovebox filled with a nitrogen atmosphere and stirred overnight. The resulting dark orange−red solution was diluted with *n*-hexane to precipitate out 2,3,5,6-tetrachlorobenzene-1,4-diol, which was filtered through a syringe filter. Removal of the solvent gave **3a** (13 mg, 83%) as a red solid. MS (matrix-assisted laser desorption/ionization (MALDI) TOF) m/z: M^+ Calcd for $C_{49}H_{29}$ 617.2; Found 617.6. Because of the limited stability of **3a** under ambient conditions, it was not possible to acquire an HRMS spectrum, and only a routine MALDI-TOF-MS spectrum was recorded. The structure of this compound was, however, unambiguously confirmed by single-crystal X-ray diffraction analysis.

*(±)-7,9,11,13-Tetraphenyl-7H-naphtho[3,2,1,8-pqra]perylen-7-ol (**12**).* A dark red solution of **3a** (6 mg, 0.01 mmol) in DCM was exposed to air, and the color changed to orange within 3−5 min. The resulting orange crude mixture was purified by column chromatography over silica gel using cyclohexane/CH_2Cl_2 (1:1) as an eluent to afford the desired product (4.2 mg, 69%) as an orange solid. ^{1}H NMR (500 MHz, CD_2Cl_2, ppm): δ 9.06 (ddd, J = 7.9, 1.0, 1.0 Hz, 1H), 8.93 (ddd, J = 8.0, 1.2, 0.6 Hz, 1H), 8.27 (d, J = 1.8 Hz, 1H), 8.13 (dd, J = 7.8, 1.0 Hz, 1H), 8.06 (d, J = 1.8 Hz, 1H), 8.02 (dd, J = 7.5, 1.1 Hz, 1H), 8.02 (dd, J = 7.8, 7.8 Hz, 1H), 7.83 (dd, J = 8.1, 7.5 Hz, 1H), 7.66 (s, 1H), 7.65−7.55 (m, 9H), 7.54−7.50 (m, 2H), 7.49−7.44 (m, 1H), 7.44−7.38 (m, 4H), 7.35−7.30 (m, 1H), 7.21−7.16 (m, 2H), 7.14−7.10 (m, 1H), 3.34 (s, 1H). ^{13}C{^{1}H} NMR (101 MHz, CD_2Cl_2, ppm): δ 151.2, 142.2, 142.0, 141.3, 141.2, 140.1, 139.18, 139.16, 137.7, 131.9, 131.8, 131.6, 130.9, 130.33, 130.30, 129.5, 129.2, 129.0, 128.83, 128.76, 128.5, 128.20, 128.16, 128.0, 127.9, 127.8, 126.96, 126.95 (2×), 126.6, 125.5, 125.4, 125.24, 125.22, 125.0, 124.8, 123.3, 122.3, 122.2, 121.9, 75.7. HRMS (ESI-TOF) m/z: $[M + Na]^+$ Calcd for $C_{49}H_{30}ONa$ 657.2189; Found 657.2187.

Quantum Chemical Calculations. All DFT calculations were performed in Gaussian 09 (Revision D.01) suite of electronic structure programs. Geometries were optimized using (U)B3LYP functional and 6-31G(d,p) basis set in the gas phase. Chemcraft software was used to analyze the TD-DFT calculated spectra and to generate graphical images of frontier molecular orbitals (FMOs). The nucleus-independent chemical shift (NICS) calculations were performed on B3LYP/6-31G(d,p) optimized geometries at the GIAO-B3LYP/6-31G(d,p) level. NICS(1) values were obtained by placing dummy atoms 1 Å above each benzenoid ring.

Single-Crystal X-ray Diffraction (XRD). Single crystals of **3a** were grown by a slow diffusion of *n*-hexane into a solution of **3a** in DCM in a glovebox (N_2). Single crystals of **12** were grown by slow evaporation of a solution of **12** in $CDCl_3$ in an NMR tube. Diffraction data were collected at 160(1) K on a Rigaku OD XtaLAB Synergy, Dualflex, Pilatus 200 K diffractometer[20] using a single-wavelength X-ray source (Cu Kα radiation: λ = 1.541 84 Å for **3a**; Mo Kα radiation: λ = 0.710 73 Å for **12**) from a microfocus sealed X-ray tube and an Oxford liquid-nitrogen Cryostream cooler. The selected suitable single crystal was mounted using polybutene oil on a flexible loop fixed on a goniometer head and immediately transferred to the diffractometer. Pre-experiment, data collection, data reduction, and analytical absorption correction[21] were performed with the program suite *CrysAlisPro*.[22] With *Olex2*,[23] the structure was solved with the *SHELXT*[24] small-molecule structure solution program and refined with the *SHELXL*-2018/3 program package[25] by full-matrix least-squares minimization on F^2. For more details about the data

DOI: 10.1021/acs.joc.9b02163
J. Org. Chem. 2020, 85, 92−100

collection and refinement parameters of both compounds, see the corresponding CIF files in the Supporting Information. Both structures were analyzed using Mercury.[26] The crystallographic views of the solid-state structures are shown in Figures 3 (**3a** and **12**), S1, and S2 (**3a**). The crystal parameters and structure refinements are summarized below. The crystallographic parameters were deposited with the Cambridge Crystallographic Data Centre (CCDC).

Crystal Parameters for Compound ***3a***. $C_{49}H_{29}\cdot 0.2(C_6H_{14})$ (M = 634.95 g mol^{-1}); red plate, 0.16 × 0.06 × 0.03 mm; monoclinic, space group $P2_1/c$ (No. 14); a = 14.5222(2) Å, b = 5.651 00(10) Å, c = 40.0027(5) Å, β = 90.9730(10)°, V = 3282.35(8) Å^3, Z = 4, T = 160.00(10) K, μ(Cu Kα) = 0.553 mm^{-1}, ρ_{calc} = 1.285 g cm^{-3}, 38 709 reflections measured (7.5° ≤ 2Θ ≤ 149.0°), 6683 unique (R_{int} = 0.0229, R_{sigma} = 0.0175), which were used in all calculations. The final R_1 was 0.0503 ($I > 2\sigma(I)$), and wR_2 was 0.1439 (all data). CCDC No. 1880918.

Crystal Parameters for Compound ***12***. $C_{49}H_{30}O$ (M = 634.73 g mol^{-1}); orange block, 0.38 × 0.31 × 0.19 mm; monoclinic, space group $P2_1/c$ (No. 14), a = 12.6312(3) Å, b = 15.7637(4) Å, c = 16.8507(5) Å, β = 107.622(3)°, V = 3197.76(15) Å^3, Z = 4, T = 160(1) K, μ(Mo Kα) = 0.077 mm^{-1}, ρ_{calc} = 1.318 g cm^{-3}, 45 969 reflections measured (4.3° ≤ 2Θ ≤ 61.0°), 9738 unique (R_{int} = 0.0319, R_{sigma} = 0.0264), which were used in all calculations. The final R_1 was 0.0467 ($I > 2\sigma(I)$), and wR_2 was 0.1356 (all data). CCDC No. 1880919.

■ ASSOCIATED CONTENT

Supporting Information

The Supporting Information is available free of charge on the ACS Publications website at DOI: 10.1021/acs.joc.9b02163.

XRD, EPR, NMR, DFT, and MS data (PDF)

Crystallographic data for **3a** (CIF)

Crystallographic data for **12** (CIF)

■ AUTHOR INFORMATION

Corresponding Authors

*E-mail: princekumar.ravat@uni-wuerzburg.de. (P.R.)

*E-mail: michal.juricek@chem.uzh.ch. (M.J.)

ORCID

Prince Ravat: 0000-0002-7553-9188

Michal Juríček: 0000-0001-5595-431X

Notes

The authors declare no competing financial interest.

■ ACKNOWLEDGMENTS

This project has received funding from the European Research Council (ERC) under the European Union's Horizon 2020 research and innovation programme (Grant No. 716139), the Swiss National Science Foundation (SNSF, M.J./PZ00P2_148043 and PP00P2_170534), the Novartis University of Basel Excellence Scholarship (P.R. and M.J.), and Julius-Maximilians-Universität Würzburg within the "Excellent Ideas" programme (P.R.). We thank Prof. C. Lambert and M. Moos for performing the CV measurements at the Univ. of Würzburg and Prof. M. Mayor for a generous support of our research at the Univ. of Basel.

■ REFERENCES

(1) (a) Su, J.; Telychko, M.; Hu, P.; Macam, G.; Mutombo, P.; Zhang, H.; Bao, Y.; Cheng, F.; Huang, Z.-Q.; Qiu, Z.; Tan, S. J. R.; Lin, H.; Jelínek, P.; Chuang, F.-C.; Wu, J.; Lu, J. Atomically Precise Bottom-Up Synthesis of π-Extended [5]Triangulene. *Sci. Adv.* **2019**, *5*, eaav7717. (b) Mishra, S.; Beyer, D.; Eimre, K.; Liu, J.; Berger, R.; Gröning, O.; Pignedoli, C. A.; Müllen, K.; Fasel, R.; Feng, X.; Ruffieux, P. Synthesis and Characterization of π-Extended Triangulene. *J. Am. Chem. Soc.* **2019**, *141*, 10621−10625. (c) Sandoval-Salinas, M. E.; Carreras, A.; Casanova, D. Triangular Graphene Nanofragments: Open-Shell Character and Doping. *Phys. Chem. Chem. Phys.* **2019**, *21*, 9069−9076. (d) Pavliček, N.; Mistry, A.; Majzik, Z.; Moll, N.; Meyer, G.; Fox, D. J.; Gross, L. Synthesis and Characterization of Triangulene. *Nat. Nanotechnol.* **2017**, *12*, 308−311. (e) Morita, Y.; Suzuki, S.; Sato, K.; Takui, T. Synthetic Organic Spin Chemistry for Structurally Well-Defined Open-Shell Graphene Fragments. *Nat. Chem.* **2011**, *3*, 197−204.

(2) (a) Gu, Y.; Wu, X.; Gopalakrishna, T. Y.; Phan, H.; Wu, J. Graphene-Like Molecules with Four Zigzag Edges. *Angew. Chem., Int. Ed.* **2018**, *57*, 6541−6545. (b) Ajayakumar, M. R.; Fu, Y.; Ma, J.; Hennersdorf, F.; Komber, H.; Weigand, J. J.; Alfonsov, A.; Popov, A. A.; Berger, R.; Liu, J.; Müllen, K.; Feng, X. Toward Full Zigzag-Edged Nanographenes: peri-Tetracene and Its Corresponding Circumanthracene. *J. Am. Chem. Soc.* **2018**, *140*, 6240−6244. (c) Ruffieux, P.; Wang, S.; Yang, B.; Sánchez-Sánchez, C.; Liu, J.; Dienel, T.; Talirz, L.; Shinde, P.; Pignedoli, C. A.; Passerone, D.; Dumslaff, T.; Feng, X.; Müllen, K.; Fasel, R. On-Surface Synthesis of Graphene Nanoribbons with Zigzag Edge Topology. *Nature* **2016**, *531*, 489−492.

(3) (a) Slota, M.; Keerthi, A.; Myers, W. K.; Tretyakov, E.; Baumgarten, M.; Ardavan, A.; Sadeghi, H.; Lambert, C. J.; Narita, A.; Müllen, K.; Bogani, L. Magnetic Edge States and Coherent Manipulation of Graphene Nanoribbons. *Nature* **2018**, *557*, 691−695. (b) Bullard, Z.; Girão, E. C.; Owens, J. R.; Shelton, W. A.; Meunier, V. Improved All-Carbon Spintronic Device Design. *Sci. Rep.* **2015**, *5*, 7634−7634. (c) Yazyev, O. V. Emergence of Magnetism in Graphene Materials and Nanostructures. *Rep. Prog. Phys.* **2010**, *73*, 056501.

(4) Nakazawa, S.; Nishida, S.; Sato, K.; Toyota, K.; Shiomi, D.; Morita, Y.; Sugisaki, K.; Hosseini, E.; Maruyama, K.; Yamamoto, S.; Kitagawa, M.; Takui, T. Molecular Spin Qubits: Molecular Optimization of Synthetic Spin Qubits, Molecular Spin AQC and Ensemble Spin Manipulation Technology. In *Principles and Methods of Quantum Information Technologies;* Yamamoto, Y., Semba, K., Eds.; Springer: Japan, 2016; Vol. *911*, pp 605−624.

(5) (a) Ravat, P.; Borozdina, Y.; Ito, Y.; Enkelmann, V.; Baumgarten, M. Crystal Engineering of Tolane Bridged Nitronyl Nitroxide Biradicals: Candidates for Quantum Magnets. *Cryst. Growth Des.* **2014**, *14*, 5840−5846. (b) Troiani, F.; Affronte, M. Molecular Spins for Quantum Information Technologies. *Chem. Soc. Rev.* **2011**, *40*, 3119−3129. (c) Sato, K.; Nakazawa, S.; Rahimi, R.; Ise, T.; Nishida, S.; Yoshino, T.; Mori, N.; Toyota, K.; Shiomi, D.; Yakiyama, Y.; Morita, Y.; Kitagawa, M.; Nakasuji, K.; Nakahara, M.; Hara, H.; Carl, P.; Hofer, P.; Takui, T. Molecular Electron-Spin Quantum Computers and Quantum Information Processing: Pulse-Based Electron Magnetic Resonance Spin Technology Applied to Matter Spin-Qubits. *J. Mater. Chem.* **2009**, *19*, 3739−3754.

(6) (a) Kubo, T. Phenalenyl-Based Open-Shell Polycyclic Aromatic Hydrocarbons. *Chem. Rec.* **2015**, *15*, 218−232. (b) Wolinska-Mocydlarz, J.; Canonne, P.; Leitch, L. C. Synthesis of 2,5,8-Trimethylphenalene. *Synthesis* **1974**, *1974*, 566−568. (c) Reid, D. H. Stable π-Electron Systems and New Aromatic Structures. *Tetrahedron* **1958**, *3*, 339−352.

(7) (a) Goto, K.; Kubo, T.; Yamamoto, K.; Nakasuji, K.; Sato, K.; Shiomi, D.; Takui, T.; Kubota, M.; Kobayashi, T.; Yakusi, K.; Ouyang, J. Y. A Stable Neutral Hydrocarbon Radical: Synthesis, Crystal Structure, and Physical Properties of 2,5,8-Tri-tert-Butyl-Phenalenyl. *J. Am. Chem. Soc.* **1999**, *121*, 1619−1620. (b) Gerson, F. Notiz Über Das ESR.-Spektrum des Phenalenyl-Radikals. *Helv. Chim. Acta* **1966**, *49*, 1463−1467.

(8) (a) Mou, Z.; Uchida, K.; Kubo, T.; Kertesz, M. Evidence of σ- and π-Dimerization in a Series of Phenalenyls. *J. Am. Chem. Soc.* **2014**, *136*, 18009−18022. (b) Small, D.; Rosokha, S. V.; Kochi, J. K.; Head-Gordon, M. Characterizing the Dimerizations of Phenalenyl Radicals by Ab Initio Calculations and Spectroscopy: σ-Bond Formation versus Resonance π-Stabilization. *J. Phys. Chem. A* **2005**, *109*, 11261−11267.

DOI: 10.1021/acs.joc.9b02163
J. Org. Chem. 2020, 85, 92−100

(9) (a) Uchida, K.; Mou, Z.; Kertesz, M.; Kubo, T. Fluxional σ-Bonds of the 2,5,8-Trimethylphenalenyl Dimer: Direct Observation of the Sixfold σ-Bond Shift via a π-Dimer. *J. Am. Chem. Soc.* **2016**, *138*, 4665−4672. (b) Uchida, K.; Hirao, Y.; Kurata, H.; Kubo, T.; Hatano, S.; Inoue, K. Dual Association Modes of the 2,5,8-Tris-(pentafluorophenyl)phenalenyl Radical. *Chem. - Asian J.* **2014**, *9*, 1823−1829.

(10) (a) Clar, E.; Stewart, D. G. Aromatic Hydrocarbons. LXVIII. Triangulene Derivatives. Part II. *J. Am. Chem. Soc.* **1954**, *76*, 3504−3507. (b) Clar, E.; Stewart, D. G. Aromatic Hydrocarbons. LXV. Triangulene Derivatives. *J. Am. Chem. Soc.* **1953**, *75*, 2667−2672.

(11) (a) Fukui, K.; Inoue, J.; Kubo, T.; Nakazawa, S.; Aoki, T.; Morita, Y.; Yamamoto, K.; Sato, K.; Shiomi, D.; Nakasuji, K.; Takui, T. The First Non-Kekulé Polynuclear Aromatic High-Spin Hydrocarbon: Generation of a Triangulene Derivative and Band Structure Calculation of Triangulene-Based High-Spin Hydrocarbons. *Synth. Met.* **2001**, *121*, 1824−1825. (b) Inoue, J.; Fukui, K.; Kubo, T.; Nakazawa, S.; Sato, K.; Shiomi, D.; Morita, Y.; Yamamoto, K.; Takui, T.; Nakasuji, K. The First Detection of a Clar's hydrocarbon, 2,6,10-Tri-tert-Butyltriangulene: A Ground-State Triplet of Non-Kekulé Polynuclear Benzenoid Hydrocarbon. *J. Am. Chem. Soc.* **2001**, *123*, 12702−12703.

(12) (a) Ravat, P.; Hinkelmann, R.; Steinebrunner, D.; Prescimone, A.; Bodoky, I.; Juríček, M. Configurational Stability of [5]Helicenes. *Org. Lett.* **2017**, *19*, 3707−3710. (b) Rickhaus, M.; Mayor, M.; Juríček, M. Strain-Induced Helical Chirality in Polyaromatic Systems. *Chem. Soc. Rev.* **2016**, *45*, 1542−1556.

(13) Ravat, P.; Ribar, P.; Rickhaus, M.; Häussinger, D.; Neuburger, M.; Juríček, M. Spin-Delocalization in a Helical Open-Shell Hydrocarbon. *J. Org. Chem.* **2016**, *81*, 12303−12317.

(14) Palewska, K.; Chojnacki, H. A Possible Mechanism of Reversible Photocyclization of [5]-Helicene in Shpol'skii-Type Matrices at 4.2 K. *J. Mol. Struct.* **2002**, *611*, 23−32.

(15) (a) Ravat, P.; Šolomek, T.; Häussinger, D.; Blacque, O.; Juríček, M. Dimethylcethrene: A Chiroptical Diradicaloid Photoswitch. *J. Am. Chem. Soc.* **2018**, *140*, 10839−10847. (b) Šolomek, T.; Ravat, P.; Mou, Z.; Kertesz, M.; Juríček, M. Cethrene: The Chameleon of Woodward−Hoffmann Rules. *J. Org. Chem.* **2018**, *83*, 4769−4774. (c) Ravat, P.; Šolomek, T.; Rickhaus, M.; Häussinger, D.; Neuburger, M.; Baumgarten, M.; Juríček, M. Cethrene: A Helically Chiral Biradicaloid Isomer of Heptazethrene. *Angew. Chem., Int. Ed.* **2016**, *55*, 1183−1186.

(16) Zaitsev, V.; Rosokha, S. V.; Head-Gordon, M.; Kochi, J. K. Steric Modulations in the Reversible Dimerizations of Phenalenyl Radicals via Unusually Weak Carbon-Centered π- and σ-Bonds. *J. Org. Chem.* **2006**, *71*, 520−526.

(17) (a) Solà, M. Forty Years of Clar's Aromatic π-Sextet Rule. *Front. Chem.* **2013**, *1*, 22−22. (b) Randić, M. Aromaticity of Polycyclic Conjugated Hydrocarbons. *Chem. Rev.* **2003**, *103*, 3449−3606. (c) Clar, E.; Macpherson, I. A. The Significance of Kekulé Structures for the Stability of Aromatic Systems—II. *Tetrahedron* **1962**, *18*, 1411−1416.

(18) (a) Liao, P.; Itkis, M. E.; Oakley, R. T.; Tham, F. S.; Haddon, R. C. Light-Mediated C−C σ-Bond Driven Crystallization of a Phenalenyl Radical Dimer. *J. Am. Chem. Soc.* **2004**, *126*, 14297−14302. (b) Koutentis, P. A.; Chen, Y.; Cao, Y.; Best, T. P.; Itkis, M. E.; Beer, L.; Oakley, R. T.; Cordes, A. W.; Brock, C. P.; Haddon, R. C. Perchlorophenalenyl Radical. *J. Am. Chem. Soc.* **2001**, *123*, 3864−3871.

(19) Fulmer, G. R.; Miller, A. J. M.; Sherden, N. H.; Gottlieb, H. E.; Nudelman, A.; Stoltz, B. M.; Bercaw, J. E.; Goldberg, K. I. NMR Chemical Shifts of Trace Impurities: Common Laboratory Solvents, Organics, and Gases in Deuterated Solvents Relevant to the Organometallic Chemist. *Organometallics* **2010**, *29*, 2176−2179.

(20) Rigaku Oxford Diffraction, 2017.

(21) Clark, R. C.; Reid, J. S. The Analytical Calculation of Absorption in Multifaceted Crystals. *Acta Crystallogr., Sect. A: Found. Crystallogr.* **1995**, *51*, 887−897.

(22) *CrysAlisPro,* version 1.171.39.13a; Rigaku Oxford Diffraction, 2016.

(23) Dolomanov, O. V.; Bourhis, L. J.; Gildea, R. J.; Howard, J. A. K.; Puschmann, H. OLEX2: A Complete Structure Solution, Refinement and Analysis Program. *J. Appl. Crystallogr.* **2009**, *42*, 339−341.

(24) Sheldrick, G. SHELXT - Integrated Space-Group and Crystal-Structure Determination. *Acta Crystallogr., Sect. A: Found. Adv.* **2015**, *71*, 3−8.

(25) Sheldrick, G. Crystal Structure Refinement with SHELXL. *Acta Crystallogr., Sect. C: Struct. Chem.* **2015**, *71*, 3−8.

(26) Macrae, C. F.; Edgington, P. R.; McCabe, P.; Pidcock, E.; Shields, G. P.; Taylor, R.; Towler, M.; van de Streek, J. Mercury: Visualization and Analysis of Crystal Structures. *J. Appl. Crystallogr.* **2006**, *39*, 453−457.

DOI: 10.1021/acs.joc.9b02163
J. Org. Chem. 2020, 85, 92−100